THE COUPLING OF FINITE ELEMENT AND INTEGRAL IQUA'I'1ON REPRESENTATIONS FOR EFFICIENT THREE-DIMENSIONAL MODELING OF ELECTROMAGNETIC SCATTERING AND RADIATION

Tom Cwik, Cinzia Zuffada, and Vahraz Jamnejad

Jet Propulsion Laboratory

California Institute of Technology

Pasadena CA 91109

1. INTRODUCTION

Finite element modeling has proven useful for accurately simulating scattered or radiated fields from complex three-dimensional objects whose geometry varies on the scale of a fraction of a wavelength. In order to make this modeling practical for engineering design, it is necessary to integrate the stages of geometry modeling and mesh generation, numerical solution of the fields, and display of field information. The stages of geometry modeling, mesh generation, and field display are commonly completed using commercially available software. packages. Algorithms for the numerical solution of the. fields need to be. written for the. specific class of problems considered. Interior problems- simulating fields in wave.gai(ics

1

and cavities- have been successfully solved using finite element methods because a bounding surface, such as the cavity walls, exactly truncates the problem domain. Exterior problems- simulating fields scattered or radiated from structures- are more difficult to model because of the need to numerically truncate the finite element mesh. To practically compute a solution to exterior problems, the domain must be truncated at some finite, surface where. the Sommerfeld radi at ion condition is enforced, either approximately or exactly. Approximate methods attempt to truncate the mesh using only local field information at each grid point, whereas exact methods are global, needing information from the entire mesh boundary. This paper outlines a method that couples three-dimensional finite element solutions interior to the. bounding surface. with an efficient integral equation solution that exactly enforces the Sommerfeld radiation condition.

A finite element model of Maxwell's equations furnishes a local solution of fields that is accurate in and around inhomogenous, complex bodies (Silvester and Ferrari, 1990; Jin, 1993). The finite element discretization can be applied to the vector Helmholtz wave equation, derived directly from Maxwell's car] equations, or to a set of equations derived from a scalar-vector potential formulation of the fields. The use of one or the other is directly tied to the choice of three-dimensional vector finite element basis functions. Edge elements (Mur and de Hoop, 1985; 1.ee and Mittra, 1992) can be naturally used to discretize the Helmholtz equation, providing tangential field continuity across material interfaces, correct discontinuitiy in normal field components across interfaces, and a natural discretization of tangential field components at geometry surfaces. Nodal elements arc. used to discretize scalar-vector potential formulations where auxiliary equations are introduced to enforce boundary conditions at surfaces and to enforce zero divergence of fields in source-

free media (Paulsen, Boyse and Lynch, **1992;** Angelini, Soize and Soudais, 1993). Formulations based on the use of mixed elements arc also possible (Mur, 1993).

Since the finite element formulation of Maxwell's equations applies to an infinite. domain, it is necessary to truncate the finite clement mesh, enforcing the Sommerfeld radiation condition. Approximate absorbing boundary conditions can be used to provide a computationally efficient enforcement of the radiation condition (Mittra, Ramahi, Khebir, Gordon and Kouki, 1989; IJ'Angelo and Mayergoyz., 1989; Chatterjee, Jin and Volakis, 1993). These boundary conditions only require local field information and therefore do not disturb the sparsity of the rc.suiting system of linear equations. Due to the inherent approximations in the enforcement of these boundary conditions however, problems can arise. in their USC. Fundamentally, they are most accurate when placed far from the object, requiring additional mesh discretization and resulting computational cost.

An alternative to approximate radiation conditions is the use of an exact expression for the fields on and outside an arbitrary sul-face that truncates the computational mesh. The. problem domain is divided into interior and exterior regions, separate.d at the mesh boundary. The interior fields are modeled using the. finite clement representat ion, while those in the exterior region are modeled using an integral equation formulation. The unknown sources in the integral equation are directly related to the tangential fields on the mesh boundary, and the radiation condition is implicitly enforced exactly through the use of the free-spacx Green's function. Fields in the two regions arc. coupled by enforcing boundary conditions cm tangential field components at the. mesh boundary, thereby producing a unique and exact solution to Maxwell's equations in both regions. One early use of this technique was outlined by Zienkiewicz, Helly and Bettess (1977). To enforce

continuity of fields at the mesh boundary, the expansion functions used in the integral equation can be identical or similar to those used at the boundary of the finite element mesh. This approach allows the mesh to conform to the body and results in a near exact enforcement of field continuity between the two regions (Angelini, Soize and Soudais, 1993; Jin and Liepa, 1988; Calalo, Imbriale, Jacobi, Liewer et al, 1989; Gong and Glisson, 1990; Yuan, Lynch and Strohbehn, 1990). It also results in the computer storage and solution time being at least proportional to that of a three-dimensional surface integral equation formulation, defeating the computational efficiency of the finite element method and limiting its usefulness.

A second approach decouples the interior finite element mesh from that used for the expansion functions in the integral equation formulation. The advantage of mesh decoupling is that a proper choice of the boundary can lead to an efficient numerical solution. In the unimoment method introduced by Mei (1972), the boundary is the surface of a separable coordinate system (for example the surface of a sphere). In the method introduced by Boyse and Seidl (] 99]) a surface of revolution is proposed which results in eigenfunction series expansion in only one direction (azimuthal). This formulation suggested a node-based tetrahedral expansion in the finite element region, and a Fourier modal azimuthal expansion together with Hermite polynomial functions along the surface of revolution generator for the integral equation expansion. A similar two-dimensional formulation for arbitrary scatterers was given by Cwi k (1992). The general three-dimensional formulation in this chapter builds upon these. previous two works, utilizing vector edge elements to discretize the Helmholtz wave equation, and piecewise triangle functions along the generator to efficiently model the mesh truncation surf ace.. The vector edge elements naturally enforce. the boundary

condition at perfectly conducting surfaces anti do not allow the generation of parasitic fields encountered when applying nodal elements. They also produce fewer non-zero entries in the resultant sparse system of equations relative to nodal elements. This approach is followed, utilizing these specific features:

1) The integral equation mesh is separate from the finite clement mesh, and its density can vary according to experienced guidelines of known integral equation solutions, independent of the finite element grid. The integral equation mesh can be as close as possible to the object, limiting the computational expense. of both the integral equation and finite element portions of the calculation.

2) The surface which truncates the finite element mesh is a surface of revolution (Boyse and Seidl, 1991). The use of this surface gives an efficient integral equation representation for the exterior fields. Using this surface decreases the. number of unknowns associated with the integral equation portion of the problem. Additionally. the surface needs only enclose the body and can be placed as close as possible to it, thus reducing the size of the problem domain.

3) Vector edge elements arc used to discretize the Helmholtz wave equation. As noted above, these functions naturally enforce the proper continuity and discontinuities in vector field components at interfaces. They also naturally enforce the boundary condition at perfectly conducting surfaces and do not

allow the generation of parasitic fields encountered when applying nodal elements.

The formulation handles both scattering and radiation problems (e.g., antenna elements or arrays). The radiation problem only differs by the need to model impressed sources by the finite element mesh (Zuffada, Cwik and Jamnejad, 1995). 10 this chapter a detailed description of the scattering formulation will be outlined, followed by an examination of convergence and accuracy, and results for a set of simple scatterers. in Cwik, Zuffada and Jamnejad (1995) further results of this approach can **be** found.

2. Theoretical formulation

The scatterer and surrounding space arc broken into two regions: an interior part containing the scatterers and freespace region oat to a defined surface, and the exterior homogenous part (Figure 1). To efficiently model fields in the exterior region, the surface bounding the interior is prescribed to be a sat-face of revolution, The following formulation first outlines the interior finite element representation, then the exterior integral equation model, and finally tbc coupling of fields at the boundary separating the two regions.

2.1 The finite element representation

In the interior region, a finite element discretization of a form of the wave equation is used to model the geometry and fields. Applying a form of Green's theorem multiplying the wave equation by a testing function $\bar{T}$, integrating over

the volume and using the divergence theorem-a weak form of the wave equation is obtained. This form includes a surface integral which provides for a boundary condition relating the field inside the selected volume to the field on the boundary, and thus provides a link to the outside field

$$\frac{\eta_0}{jk_0}\iiint_V\left[\frac{1}{\varepsilon_r}\left(\nabla\times\overline{H}\right)\bullet\left(\nabla\times\overline{T}^*\right)-k^2\mu_r\overline{H}\bullet\overline{T}^*\right]dv-\iint_{\partial V}\overline{E}\times\hat{n}\bullet\overline{T}^*ds=0 .$$

(1)

$\overline{H}$ is the magnetic field (the $\overline{H}$-equation is used in the development; the formulation of the dual $\overline{E}$-equation is presented in Section 5), $\overline{T}$ is a testing function, the asterisk denotes conjugation, and $\overline{E}\times\hat{n}$ is the tangential component of $\overline{E}$ on the surface S (∂V). In general, ∂V represents all boundaries of the volume, including the surface of revolution and any perfect conductors. The surface integrals over the perfect conductors are identically zero since their integrand includes the tangential electric field $\overline{E}\times\hat{n}$. Equation (1) therefore represents the fields internal to and on the surface S. These fields will be modeled using a set of properly chosen finite element basis functions. in Equation (1), ε_r and μ_r are the relative permittivity and permeability respectively, and k_0 and η_0 are free.-space wave number and impedance, respectively.

2.2 The combined-field integral equation representation

In the formulation of the integral equation, fictitious electric $\left(\overline{J}=\hat{n}\times\overline{H}\right)$ and magnetic $\overline{M}=-\hat{n}\times\overline{E}$) surface currents, equivalent to the tangential magnetic and electric fields just on the exterior of the boundary surface, arc defined

on the boundary. These currents produce fields in the exterior region which are the scattered fields. The sum of the scattered and the incident field results in the total field everywhere outside the boundary surface. On the boundary itself, this sum is equal to half the total field. The scattered fields are obtained from the tangential currents via an integral over the boundary using the free-space Green's function kernel. Two equations are obtained for the electric and magnetic fields on the boundary- the electric field integral equation (EFIE) and the magnetic field integral equation (MFIE), respectively. A linear combination of the two with a constant weighting factor α results in the combined field integral equation (CFIE). The general form used in this formulation is

$$Z_M[M/\eta_0] + Z_J[J] = V_i \tag{2}$$

where Z_M and Z_J are the integro-differential operators used in defining the CFIE, and V_i represents the incident field.

2.3 Enforcing boundary conditions

The previous two sections have outlined field representations for the interior and exterior regions. In the interior region, boundary conditions al any material interface, including perfect conductors, must be enforced by a proper application of the finite element basis functions. At the artificial surface of revolution separating the interior and exterior regions, boundary conditions on the continuity of tangential field components must be enforced.

Initially, four equations are written for the three unknown field quantities of interest. The first unknown is the magnetic field internal to the volume V. The other two are the electric and magnetic surface currents, J and $\overline{M}$, on the boundary.

The four equations are found from the finite element equation (1), the integral equation (CFIE) relating $\overline{J}$ and $\overline{M}$ currents to the incident field (2), and a set of equations enforcing the continuity of H and $\overline{E}$ across the boundary, Continuity of the magnetic field across the boundary is enforced in a weak sense

$$\iint_{\partial N} \left(\hat{n} \times \overline{H} - \overline{J} \right) \bullet \left(\hat{n} \times \overline{U}^* \right) ds = 0 \tag{3}$$

where. $\overline{U}$ is a testing function. This is an essential boundary condition and must be explicitly enforced. Continuity of the electric field across the boundary is made implicit in the finite element equation in the surface integral term $\hat{n} \times \overline{E}$, and is termed a natural boundary condition

$$\iint_{\partial N} \left(\overline{E} \times \hat{n} - \overline{M} \right) \bullet \overline{T}^* ds = 0 \tag{4}$$

This equation is combined with (1) to produce

$$\frac{\eta_0}{jk_0} \int_V \left[\frac{1}{\varepsilon_r} \left(\nabla \times \overline{H} \right) \bullet \left(\nabla \times \overline{T}^* \right) - k^2 \mu_r \overline{H} \bullet \overline{T}^* \right] ddv - \int_{\partial V} \overline{M} \bullet \overline{T}^* ds = 0. \tag{5}$$

Equations (5), (3) and **(2)** constitute the system of equations representing fields in all space in and about the scatterer.

3. Numerical implementation

The three equations (5), (3) and (2) are discretized using appropriate sets of basis functions. In the interior region, tetrahedral, vector edge elements (Whitney elements) are used. On the bounding surface of revolution, a set of functions with piecewise linear variation along the surface of revolution generator, and with an azimuthal Fourier modal variation are used.

3.1 The finite element model

An ensemble of elements filling the interior region, excluding any perfect conducting objects, is created using a mesh generator. The elements should accurately represent the magnetic field, the geometry of the scatterer, and the bounding surface of revolution. Since the scatterer is not a body of revolution in general, the finite element mesh will extend out from the scatterer to the surface of revolution. For an accurate model of the fields, tetrahedral, vector edge elements are used to model $\overline{H}$ (Lee and Mittra, 1992)

$$\overline{H}(r) = \sum_i h_i \overline{W}_i(r) \tag{6}$$

where

$$\overline{W}_{mn}(r) = \lambda_m(r)\nabla\lambda_n(r) - \lambda_n(r)\nabla\lambda_m(r) \tag{6a}$$

and $\lambda(r)$ are the tetrahedral shape functions. Testing functions are also chosen to be the functions $\overline{W}(r)$.

These functions are used in the volume integral of (S). The resultant discretized volume integral is

$$\frac{\eta_0}{jk_0}\int_V\left[\frac{1}{\varepsilon_r}\left(\nabla\times\overline{H}\right)\bullet\left(\nabla\times\overline{W}^*\right)-k^2\mu_r\overline{H}\bullet\overline{W}^*\right]dv\Rightarrow \mathbf{KH} \qquad (7)$$

where $\mathbf{K}$ is the assembled sparse finite element matrix, and 11 is the vector of complex, finite element basis function amplitudes.

3.2 An efficient exterior integral equation model

In the surface of revolution geometry, a cylindrical coordinate system (ρ,ϕ,z) is selected for the exterior region, and orthogonal surface coordinates (t,ϕ) are used on the boundary itself; ϕ is the azimuthal angle variable and t is the contour length variable along the generating curve of the surface of revolution. In the formulation of the integral equation, the equivalent electric and magnetic surface currents (J and M) are defined just on the outside of the surface through the. relations

$$u\overline{E} = \overline{E}^i - L[\overline{J}] + K[\overline{M}/\eta_0] \qquad (8)$$

11

$$u\eta_0\,\overline{H} = \eta_0\,\overline{H}^i - K[\overline{J}] - L[\overline{M}/\eta_0]\qquad(9)$$

in which u is the Heaviside function,

$$u = \begin{cases} 1, & \text{for points outside } \partial V \\ \frac{1}{2}, & \text{for points on } \partial V \\ 0, & \text{for points inside } \partial V \end{cases}\qquad(9a)$$

and L and A' are integro-differential operators given by

$$L[\cdots] = j\eta_0 \iint_{\partial V} \left(k_0^2\,[\cdots] + \nabla\nabla'\cdot[\cdots]\right) g(k_0|\bar{r} - \bar{r}'|)\,ds'\qquad(1\,0)$$

$$K[\cdots] = \eta_0 \iint_{\partial V} [\cdot\,\cdot] \times k_0\nabla g(k_0|\bar{r} -- \bar{r}'|)\,ds'\qquad(11)$$

In (1 0) and (11) g is the Green's function for unbounded space

$$g(k_0|\bar{r} - \bar{r}'|) = \frac{e^{-ik_0|\bar{r} - \bar{r}'|}}{4\pi k_0|\bar{r} - \bar{r}'|}.\qquad(12)$$

From the above equations we can write the following two integral equations on the tangential components of the field, for obtaining the. $\bar{J}$ and $\overline{M}$

surface currents. The electric field integral equation, and magnetic field integral equal ion respectivly arc,

$$(\tfrac{1}{2} \eta_0 \, \hat{n} \times I - K)[\overline{M} / \eta_0]\big|_{\text{tan}} + L[\bar{J}]\big|_{\text{tan}} = \hat{n} \times \overline{M}_i, \qquad (13a)$$

$$(\hat{n} \times L) \, [\overline{M} / \eta_0] + (\tfrac{1}{2} \eta_0 \, I + \hat{n} \times K)[\bar{J}] = \eta_0 \, \bar{J}_i, \qquad (13b)$$

in which, for the sake of symmetry, the source term (tangential components of the incident field) arc given as fictitious surface currents $\bar{J}_i$ and $\overline{M}_i$. "I'hey arc presented in a form that is very similar both in terms of dimensions as well as vector orientations. The symbol, 1, represents the unity operator and is introduced for notational consistency.

These two integral equationse arc linearly combined to obtain the combined-field integral equation

$$\left\{(1 - \alpha)(\tfrac{1}{2} \eta_0 \, \hat{n} \times I - K) + \alpha \, (\hat{n} \times L)\right\} [\overline{M} / \eta_0] +$$
$$\left\{(1 - \alpha) L + \alpha \, (\tfrac{1}{2} \eta_0 \, I + \hat{n} \times K)\right\}[\bar{J}] = \qquad (14)$$
$$(1 - \alpha)\hat{n} \times \overline{M}_i + \alpha \, \eta_0 \, \bar{J}_i$$

1 :quat ion (14) is put in the more compact form given by (2) where the operators

$$Z_M = \left\{(1 - \alpha)(\tfrac{1}{2} \eta_0 \, \hat{n} \times I - K) + \alpha \, (\hat{n} \times L)\right\}$$

$$Z_J = \left\{ (1 - \alpha)L + \alpha \left(\tfrac{1}{2} \eta_0 \, I + \hat{n} \times K \right) \right\} \tag{15}$$

and source term

$$\overline{V}_i = (1 - \alpha)\hat{n} \times \overline{M}_i + \alpha \eta_o \overline{J}_i \tag{16}$$

are used. This formulation of the operators follows from CICERO code development (Medgeysi-Mitschang and Putnam, 1984), although other formulations are also possible.

Using the method of moments, this integral equation is turned into a matrix equation. The unknown currents $\overline{M}$ and J are expanded in a finite series of basis functions $\overline{U}$ on the surface of revolution. The testing functions are selected identical to expansion functions on the surface of revolution. They are written as separable functions of t and ϕ and will have two orthogonal components along the $\hat{t}$ and $\hat{\phi}$ directions. The azimuthal function is the exponential harmonic $\exp(jn\phi)$ (Fourier harmonics). The variation along the surface of revolution generator is represented by a triangle function $T(t)$ divided by $\rho(t)$, the radial distance from the z-axis. Thus,

$$\overline{J} = \sum_{n,k} \left(a_{n,k}^t \, \overline{U}_{n,k}^t - a_{n,k}^\phi \, \overline{U}_{n,k}^\phi \right) \qquad in \; \partial V \tag{17}$$

$$\overline{M} = \sum_{n,k} \eta_0 \left(b_{n,k}^t \, \overline{U}_{n,k}^t - b_{n,k}^\phi \, \overline{U}_{n,k}^\phi \right) \qquad in \; \partial V \qquad (18)$$

$$\overline{V}_i = \sum_{n,k} \left(c_{n,k}^t \, \overline{U}_{n,k}^t - c_{n,k}^\phi \, \overline{U}_{n,k}^\phi \right) \qquad in \; \partial V \qquad (19)$$

and both expansion and testing functions are given as

$$\overline{U}_{n,k}^t = \hat{t} \frac{T_k(t)}{\rho(t)} e^{jn\phi} \qquad (20)$$

$$\overline{U}_{n,k}^\phi = \hat{\phi} \frac{T_k(t)}{\rho(t)} e^{jn\phi} \qquad (21)$$

$T_k(t)$ is a triangle function spanning the k-th annulus cm the surface of revolution. Each annulus spans two segments along the generator, each referred to as a strip. Adjacent triangles overlap on one segment. These overlapping triangle functions result in approximations to $\overline{J}$ and $\overline{M}$ which are piecewise linear in t and a Fourier series in ϕ.

in the moment method, inner products are formed between the testing functions and the integral equations expanded over the basis functions. Here, using the Galerkin method, basis and testing functions are chosen identical as above.. The complex inner product between any two vectors $\overline{U}$ and $\dot{V}$ *is defined* as

15

$$\langle \overline{U}, \overline{V} \rangle_{\partial V} = \iint_{\partial V} \overline{U} \cdot \overline{V}^* ds. \tag{22}$$

The original integral equation is transformed into a set of linear equations for each of the Fourier modes since the Fourier modes are orthogonal and decouple. Thus, in the compact form it can be written as:

$$\sum_m m_m \langle Z_{Mm} [\tilde{U}_m], \overline{U}_n \rangle + \sum_m j_m \langle Z_{Jm} [\overline{U}_m], \overline{U}_n \rangle = \sum_m v_{im} \langle \overline{U}_m, \overline{U}_n \rangle$$

$$\tag{23}$$

where m_m and j_m are the complex unknown amplitudes for each Fourier mode. This is the second equation in the system, representing fields scattered from the object.

3.3 Coupling the two representations

The surface. integral in (S) and the first component of the integral in (3) are termed the coupling integrals, since with a convenient choice of the unknown in the first and of the testing function in the second, they are made to couple interior and exterior field representations, The surface S in these surface integrals is chosen to be that of the surface of revolution. Because the surface of revolution is discretized when using these basis functions, the issue arises of how to represent W on S. Indeed, the outer surface of the interior volume is a union of finite element facets. These facets vary, according to the order of finite element representation chosen, from planes to curved surfaces. In general, however, this surface is not identical to

16

the surface of revolution. Similarly, the surface of revolution is obtained by revolving a generating curve around an axis, creating a surface whose cross section is circular. However, for numerical purposes, the generator itself is not necessarily smooth, but is piecewise linear, Thus practically, only in the limit of fine meshing will the two surfaces coincide with each other.

The finite element function $\overline{W}$ is evaluated approximately on the portion of surface of revolution projected from the triangular facet of the tetrahedron onto a strip. This is accomplished by an orthogonal projection of the tetrahedral facet surface onto the surface of revolution, thus introducing an error which depends on the size of the tetrahedral facet with respect to the curvature of the surface of revolution. The coupling term is given by the integral

$$ C = \iint_{\partial V} \overline{U} \bullet \overline{W}^* ds \tag{24} $$

where, for each integral equation basis and finite element testing function, the contributing surface is the union of the projections of a triangular boundary surface onto the proper number of surface of revolution strips (up to two in well-posed cam). Such surfaces arc curved triangles, curved quadrilaterals, or curved pentagons. The evaluation of the integrals was done numerically by first inscribing the above irregular surfaces into curved rectangles and then by determining the points inside the region of interest from the knowledge of the simplex coordinates of the original finite element boundary facet and their properties at points inside the facet, These coupling integrals, as well as the discretization of the second surface integral in (3), complete the discretization of the problem.

4. Numerical solution of the linear system

having introduced the basis and testing functions for the volume as well as the surface unknowns, substitution into the complete. set of equations yields

$$\sum_{p=1}^{P} h_p \left\langle \kappa_p \left[\bar{W}_p \right] \cdot \bar{W}_q \right\rangle - \eta_0 \sum_{m=1}^{M} m_m \left\langle \bar{U}_m \cdot \bar{W}_q \right\rangle = 0, \qquad q = 1,2,3...P$$

$$-\eta_0 \sum_{p=1}^{P} h_p \left\langle \bar{W}_p \cdot \bar{U}_n \right\rangle + \eta_0 \sum_{m=1}^{M} j_m \left\langle \bar{U}_m \cdot \left[\hat{n} x \bar{U}_n \right] \right\rangle = 0, \qquad n = 1,2,3...M$$

$$\sum_{m=1}^{M} m_m \left\langle z_{Mm} \left[\bar{U}_m \right] \cdot \bar{U}_n \right\rangle + \sum_{m=1}^{M} j_m \left\langle z_{Jm} \left[\bar{U}_m \right] \cdot \bar{U}_n \right\rangle = \sum_m v_{i_m} \left\langle \bar{U}_m \cdot \bar{U}_n \right\rangle, \quad n = 1,2,3...M$$

$$(25)$$

which can be expressed in matrix form as

$$\begin{vmatrix} \mathbf{K} & \mathbf{C} & 0 \\ \mathbf{C}^{\dagger} & 0 & \mathbf{Z_0} \\ 0 & \mathbf{Z_M} & \mathbf{Z_J} \end{vmatrix} \begin{vmatrix} \mathbf{H} \\ \mathbf{M} \\ \mathbf{J} \end{vmatrix} = \begin{vmatrix} 0 \\ 0 \\ \mathbf{V_I} \end{vmatrix} \qquad (26)$$

where

$$K = \left\langle K_p \left[\overline{W}_p \right] \cdot \overline{W}_q \right\rangle$$

$$\mathbf{C} = - \eta_0 \left\langle \overline{U}_m \cdot \overline{W}_q \right\rangle$$

$$\mathbf{Z}_0 = \eta_0 \left\langle \overline{U}_m \cdot \left[\hat{n} \times \overline{U}_n \right] \right\rangle \qquad (27)$$

$$\mathbf{Z}_\mathbf{M} = \left\langle Z_{Mm} \left[\overline{U}_m \right] \cdot \overline{U}_n \right\rangle$$

$$\mathbf{Z}_\mathbf{J} = \left\langle Z_{Jm} \left[\overline{U}_m \right] \cdot \overline{U}_n \right\rangle$$

K_p is tbc volume integral operator in (7); Z_{Mm} anti Z_{Jm} arc defined in the. previous sections. Note that † indicates the adjoint of a matrix, while P and M arc the number of finite clement and integral equation basis functions, respectively.

It is noted that the overall matrix size is dominated by K since the surface unknowns arc generally a small fraction of those in the volume. Note also that both K and C are sparse, Z_0 is tri-diagonal and Z_M and Z_J arc banded. The overall matrix is very sparse and looks like the scatter plot illustrated in Figure 2 for a small problem generated for graphical demonstration. in particular it is complex, non-symmetric, and non-Hermitian.

The solution to this matrix equation has been developed using two alternat i ve strategies depending upon the application. The two approaches arc

1) Solve the entire system in one step using an iterative algorithm for non-symmetric systems. in this work the non-symmetric variant of the quasi

minimal residual algorithm (Freund and Nachtigal, 1991; Lucas, 1993) was applied.

2) Solve the system in two steps by first eliminating H through the computation of $Z_K = C^\dagger K^{-1}C$ and then by solving the reduced system

$$-Z_K M - Z_0 J = O$$
$$Z_M M + Z_J J = V_1 \text{ "}$$

(28)

The first step was accomplished by applying a symmetric variant of the quasi-minimal residual iterative algorithm as well as a direct solver based on an sparse $U^\dagger D U$ factorization. The resulting overall matrix (28) was treated as being dense and the solution of this second system was accomplished via a direct dense LU decomposition, since its size is relatively small.

The choice of the solution method is dependent upon a variety of factors, including the number of right-hand side excitation vectors and the efficacy of a preconditioner if iterative algorithms are used to calculate Z_K in the second method. The computational cost of the first method is mainly due to solving the system iteratively for each right hand side. The major computational cost in the second method is calculating Z_K ; this requires the solution of a system of equations, $K^{-1}C$, where C is a rectangular matrix with a possibly large number of

columns for electrically large scatterers. When considering a radiation problem where there are one or a few right-hand sides, or a scattering problem with one or a few excitations, the first method may be preferable. When mono-static radar cross section calculations are. performed and there are upwards of thousands of right-hand sides, the second method is more appropriate. This second approach has been implemented on scalable distributed memory computers, and is reported in Cwik, Katz, Zuffada and Jamnejad (1 995).

The speed of convergence of iterative methods such as the quasi-minimal residual algorithm depends on the condition number of the matrix. To improve on the. condition number of the matrix of (26) in a one-step solution, or of matrix K in a two-step solution. standard preconditioning methods have been examined. It is noted that, when preconditioning the original matrix, it is necessary to preserve its valuable properties–in the case of the one-step it is sparsity, whereas for the two-step approach it is sparsity and symmetry. A matrix M is used as a left preconditioner in the one-step solution

$$M \cdot A \cdot x = M \cdot b \tag{29}$$

where A is the global matrix and b is the right hand side. '1'0 preserve the sparsity of the matrix, the multiplication on the left-hand side of (29) is performed every time the matrix is used by the quasi-minimal residual algorithm, so that the algorithm operates on a sparse matrix. It is seen that the solution to the modified problem is the same as that to the original problem.

Alternately, in the two-step method, the matrix on which the quasi-minimal residual algorithm is applied is symmetric. Then the scheme of (29) is modified into the symmetric scheme

$$\underbrace{M' \cdot A \cdot M'}_{symmetric\ matrix} \cdot \left[\underbrace{\left(M' \right)^{-1} x}_{x',\ modified\ solution} \right] = M' \cdot b \tag{30}$$

where the matrix M' is a symmetric preconditioner. Again, to preserve the sparsity of the matrix, the multiplications by M' are performed every time the matrix is used by the quasi-minimal residual algorithm, so that the algorithm operates on a sparse system. More detailed information on the matrix equation solvers can be found in Cwik, Katz, Zuffada and Jamnejad (1 996).

5. Electric field formulation

A dual formulation for the electric field within the mesh can be developed by either reformulating the problem beginning with the Helmholtz equation for the electric field in Sections 2 through 4, or by applying duality to the final equations in Section 4. As in the magnetic field formulation, this formulation involves the expansion of the electric field over the mesh as

$$\overline{E}(r) = \eta_o \sum_i e_i \overline{W}_i(r) \tag{31}$$

where η_o is introduced as it was in the expansions in Section 3 to scale the equations properly. The resultant system dual to (26) then is

$$\begin{vmatrix} \mathbf{K}^E & \mathbf{C} & \mathbf{0} \\ \mathbf{C}^\dagger & 0 & -\mathbf{Z}_0 \\ 0 & \mathbf{Z}_J & \mathbf{Z}_M \end{vmatrix} \begin{vmatrix} E \\ J \\ M \end{vmatrix} = \begin{vmatrix} \mathbf{0} \\ 0 \\ V_I \end{vmatrix}$$

(32)

where $\mathbf{K}^E$ is the dual of (7)

$$\frac{\eta_0}{jk_0} \int_V \left[\frac{1}{\mu_r} \left(\nabla \times \overline{E} \right) \bullet \left(\nabla \times \overline{W}^* \right) - k^2 \varepsilon_r \overline{E} \bullet \overline{W}^* \right] dv \Rightarrow \mathbf{K}^E E$$ (33)

and other notation remains unchanged.

The electric field formulation has specific advantages when simulating the fields scattered m radiated from particular objects. For example when considering objects with perfectly conducting flat plates or fins, or objects with electrically thin strips or patches, it is more expedient to apply the perfectly conducting boundary condition using the electric field formulation than the magnetic field formulation. In the electric field formulation, element edges that lie on the perfect conductor are removed from the vector E, and the matrix block $\mathbf{K}^E$ is similar] y reduced in si ze. This has the explicit effect of zeroing the coefficients of the electric field lying on the zero thickness perfect conductors, satisfying the boundary condition that the total tangential electric field is zero on the perfect conductor. To accomplish this enforcement of the boundary conditions using the magnetic field formulation, the thin conductor must be modeled as a thin volumetric region. The ensuing mesh generation difficulties of creating the small, often distorted elements, makes this inconvenient if impractical in practice. An alternative strategy is to mcsb both faces of the zero thickness conductor with edges that are distinct, though coincident,

therefore modeling the tangential magnetic field on the both faces of the conductor. This also leads to meshing difficulties in practice.

6. Numerical convergence and results

Several scatterers have been examined in detail, including dielectric sphere.s, (coated) metal spheres, finite length (coated) metal cylinders, metal conespheres, and metal cubes. Results for the spheres and dielectric cylinders will be presented here, results for (he other objects can be found in Cwik, Zuffada and Jamnejad (1 995). The features of some of the meshes arc shown in Table 1. A surrounding shell is used to model a perfectly conducting object coated with a layer of dielectric material, As a special case, by choosing the dielectric coating to be air, the scattering from the perfectly conducting object itself is obtained. Naturally, no elements arc required to model fields inside. perfect conductors. The choice of metallic objects was based on the existence of results from other codes to be used for comparisons.

'J'able 1. Objects and their mesh densities

Object	Nodes	Elements	Edges
1 Dielectric sphere 1	865	3,963	5,217
Dielectric sphere 2	2,273	10,240	1'2,896
Metal sphere (coated)	516	1,716	2,889
Dielectric cylinder	7,076	34,776	43,791

When considering the dielectric sphere or cylinder, only the scatterer itself was modeled by the mesh since there is no need to extend the mesh outside the geometry of the scatterer. in the case of the metal sphere, the mesh was a shell conforming to the object with a thickness chosen to fit one tetrahedral element,

6.1 Numerical accuracy

The accuracy of this method, compared to analytic solutions or alternative computational methods or measurements, was investigated as a function of several parameters. Some specific parameters are:

- mesh density
- number of surface of revolution basis functions along the generator
- number of surface of revolution azimuthal Fourier modes
- electric permittivity and magnetic permeability of scatterer.

The first three are functions of electrical wavelength. It is noted that these parameters are not independent, but rather are closely related. The canonical object studied for accuracy was the sphere. Both a metal sphere and a dielectric sphere were. considered, and in the latter case, meshes of two different densities were investigated. For simplicity the direction of incidence was taken to be the positive z direction with the electric field polarized along x, and the Fourier modes (-1, O, +1) were considered. Theoretically only the +1 and -1 modes are present in the decomposition of this incident plane wave, and no other mode should arise in the scattered field. The quantity of interest was chosen to be the fields scattered in the E-

plane ($\phi = 0^0$). An error measure was constructed by taking the difference between the calculated and exact values, integrated over the range of angles of observation $0° \leq \theta \leq 180°$. This number was divided by the integral of the anal ytic solution over the same range to obtain a measure of quality for (he solution.

Table 2 illustrates tbc range of variation for some of the parameters that were. considered. The electric permittivity ε_r was fixed at 9 for the study of the dielectric sphere, whereas the metal sphere was treated with a "coating" of free space. The table illustrates that the frequency upper limit was chosen to correspond to the ratio of edges per wavelength close to 10. The choice was made with the intention to investigate the limitations of mesh applicability and to quantify errors in this rather broad range.

As seen in the following results, high accuracy was obtained for a) average wavelength to edge ratios between 2(I and 40, and b) wavelength to surface of revolution triangle length ratios bet wccn 10 and 20. Lower accuracy can be found for lesser numbers of unknowns per wavelength.

Table 2. Summary of edges per wavelength on surface of revolution

I requency (GHz)	3	5	7	10	15
Metal Sphere† (16)*	*50*	31	22	15	10
Dielectric Sphere 1†† (16)*	17	10	7	-	-
Dielectric Sphere 2†† (24)*	25	15	11	-	-

*Nominal number of edges along **generator**
†A layer of free space is meshed
††$\mathcal{E}_r = $ *9 used*

6.2 Radar cross section and near-field results

A set of radar cross section calculations, showing comparisons with either analytical results or with calculations obtained with the CICERO code, is provided in Figs. 3-7. As mentioned previously results for other objects can be found in Cwik, Zuffada and Jamnejad (1 995). in the legend our calculation is referred to as PHOEBUS, the name of the software developed from this formulation. Figure 3 illustrates the bistatic radar cross section of a metal sphere (radius = ().8 cm) coated with a layer of lossy dielectric (thickness = 0.2 cm). Calculations arc performed in both the E-plane and the H-plane and comparisons arc made with available analytical results. The frequency of excitation is 15 GHz.

Figure 4 illustrate.s the monostatic radar cross section of a dielectric cylinder (length = 10.0 cm, radius = 1.0 cm) with $\mathcal{E}_r = 4$. The comparison is made with the CICERO code for the $\phi-\phi$ plane at 2.5 GHz. The discrepancy between the two plots is due to geometry modeling using the piecewise linear finite element and sulfate, of revolution basis functions. This result used finite element tetrahedron with an average edge length of 0.2 cm. By decreasing this edge length the two curves can be made arbitrarily close. The smaller edge length better models the physical geometry, but is electrically over-sampled (greater than the '20-30 edges per wavelength typically needed). This type of modeling discrepancy is common in the finite element method when using the linear (non-isoparametric) tetrahedron functions.

27

Figure **5 illustrates** the near-field results of the electric and magnetic field on the surface of the dielectric sphere with $\mathcal{E}_r = 9$. Shown arc the $\hat{r}$ and $\hat{\phi}$ components of both E and H along a line at $\phi = 45°$. The radius of the sphere is 1 cm, and the PHOEBUS results are compared with analytical ones at 5 GHz.

7. Conclusions

This paper presents a method to compute. the fields of penetrable three-dimensional scatterers of general shape by coupling a finite element solution to an integral equation solution on a surface of revolution. The surface of revolution is chosen to surround the scatterer, resulting in a minimal amount of volume that needs to be discretized. The use of the integral equation provides an exact enforcement of the Sommerfeld radiation condition. Vector edge elements are used to discretize the fields inside the volume, whereas the integral equation is discretized on a decouple.ci surface mesh, introducing a small set of additional basis functions to the system. Scattered fields for a variety of objects have been investigated, as well as fields inside penetrable scatterers.

8. References

Angelini, J-J, Soize, C. and Soudais, 1'. (1993), "Hybrid Numerical Method for Harmonic 3-D Maxwell Equations: Scattering by a Mixed Conducting and Inhomogenous Anisotropic Dielectric Medium, " *IEEE Transactions on Antennas and Propagation*, *vol. AP-41, no. 1*, pp. 66-76, Jan.

Boyse W., and Seidl, A. (1 991), "A Hybrid Finite Element Method for Near Bodies of Revolution," *IEEE Trans. Mag, vol.* 27, pp. 3833-3836, Sept.

Calalo, R., Imbriale, W., Jacobi, N., Liewer, P., et al (1989), "Hypercube Matrix Computation 'J'ask, Research in Parallel Computational Electromagnetics, Report for 1988--J 989," Jet Propulsion Laboratory, Nov.

Chatterjee, A., Jin, J-J., and Volakis, J. (1993), "Edge-Based Finite Elements and Vector ABC's Applied to 3-D Scattering, *IEEE Transactions on Antennas and Propagation, vol. AP-41, no. 2, pp. 221-226,* I'cb.

Cwik, 'J'. (*]992*), "Coupling Finite Element and integral Equation Solutions Using Decoupled Boundary Meshes," *IEEE Trans. Antennas Propagat., vol. A P-40, no. 12,* pp. 1496-] 504, Dec.

Cwik, T., Katz, D., Zuffada, C., and Jamnejad, V. (1 995), "The Application of Scalable Distributed Memory Computers to the Finite Element Modeling of Electromagnetic Scattering and Radiation)" submitted to Computer Methods i n Applied Mechanics and Engineering.

Cwik, T., Zuffada, C., and Jamnejad, V. (199 S), "Efficient Coupling of Finite Element anti Integral Equation Representat ions to model Scat tering from Three-Dimensional Objects," submitted to IEEE Transactions on Antennas and Propagation.

D'Angelo, J., and Mayergoyz, 1. (1 989), "On the Use of Local Absorbing Boundary Conditions for RF Scattering Problems," *IEEE Transactions on Magnetics*, vol. 25, 1>1>.3040 3043> July.

Freund, R. and Nachtigal, N. (1 991), "QMR: a Quasi-Minimal Residual Method for Non-Hermitian Linear Systems," *Numerische Mathematik*, **60, pp. 315-339.**

Gong, Z., and Glisson, A. (1990), "A Hybrid Equation Approach for the Solution of Electromagnetic Scattering Problems involving Two-Dimensional Inhomogenous Dielectric Cylinders," *IEEE Trans. Antennas Propaga t., vol. AP-38*, pp. 60–68, Jan.

Jin J-J, and Liepa, V. (1 988), "Application of Hybrid Finite Element Method to Electromagnetic Scat tering from Coated Cylinders," *IEEE Trans. A ntennas and Propagat. ion, vol. AP-36, pp.* 50- *S4,* Jan.

Ji n, J-J. (1993), *The Finite Element Method in Electromagnetics,* John Wiley and Sons, Inc., New York.

Lee, J. and Mittra, R. (1 992), "A Note On The Application Of Edge-Elements For Modeling 3-Dimensional Inhomogeneously-Filled Cavities)" *IEEE Transactions On Microwave Theory and Techniques, vol.* **40, m. 9, pp. 1767-1773, Sept.**

1 ucas, E. (*1 993),* Personal Communications.

Medgeysi-Mitschang, 1... and Putnam, J. (1984), "Electromagnetic Scattering from Axially Inhomogeneous Bodies of Revolution,>' *IEEE Transactions on Antennas and Propagation, vol. AP-32, pp.* **797-806.**

Mci, K. (1972), "Unimoment method of solving antenna and scattering problems," *IEEE Transactions on Antennas and Propagat., vol. A P-22,* pp. 760-766, Nov.

Mittra, R., Ramahi, O., Khebir, A., Gordon, R., and Kouki, A. (1989), "A Review of Absorbing Boundary Conditions for Two- and Three-Ilil~lensi{Jnal 1 lect romagnetic Scat tering Problems," *IEEE Trans. Mag, vol.* 2s, *no.* 7, pp. 3034-3040, July,

Mur, G. (1993), "l'he Finite-Element Modeling of Three-Dimensional Electromagnetic Fields Using Edge and Nodal Elements, *IEEE Transactions on Antennas and Propagation, vol. AP-41, no. 7,* pp. 948-953, July.

Mar, G. and de Hoop, A. (1985), "A Finite-Element Method for Computing Three-Dimensional Electromagnetic Fields in Inhomogeneous Media," *IEEE Trans. Mag., vol.* 2], *no.* 6, pp. 2188-2191, Nov.

Paulsen, D., Boyse, W. and Lynch, D. (1992), "Continuous Potential Maxwell Solutions on Nodal -Based Finite Elements," *IEEE Transactions on A ntennas and Propagation, vol. A P-40, no. 10,* pp.1192-1 200, Ott.

Silvester, 1', and Ferrari, R. (1 990), *Finite Elements for Electrical Engineers, Second Edition,* Cambridge Press, Cambridge.

Yuan, X., Lynch, D., and Strohbehn, J. (1990), "Coupling of finite element and moment methods for electromagnetic scattering from inhomogenous objects," *IEEE Trans. Antennas Propagat., vol. AP-38*, pp. 386 394, Mar.

Zienkiewicz, ()., Kelly, D., and Bettess, P. (1 977), "The Coupling of the Finite Element Method and Boundary Solution Procedures," *Intl. Journ. Num. Meth. Engr., vol. 11,* pp. 355–375, Nov.

Zuffada, Cwik, T., and Jamnejad, V.(1 995), Modeling Radiation with an Efficient Hybrid Finite Element-Integral Equation-Wavegu ide M o d e Modeling Technique, Submitted to II EE Transactions on Antennas and Propagation.

1,1ST OF FIGURES

Figure]. Geometry of computational domain showing interior' and exterior regions.

Figure 2. Scatter plot figuratively showing structure of system of equations.

I)arkened spaces indicate non-zero matrix entries.

Figure 3. Bistatic radar cross section of coated metal sphere (radius = 0.8 cm,

coating thickness 0.2 cm) at IS GHz.

Figure 4. Bistatic radar cross section of dielectric cylinder (radius = 1 cm, height =

10 cm) at 2.5 Ghz.; ϕ–ϕ plane.

Figure 5. Electric and magnetic fields on surface of dielectric sphere. (radius= 1cm)

at 5 GHz. Both t and ϕ components are compared to analytical solutions in a cut
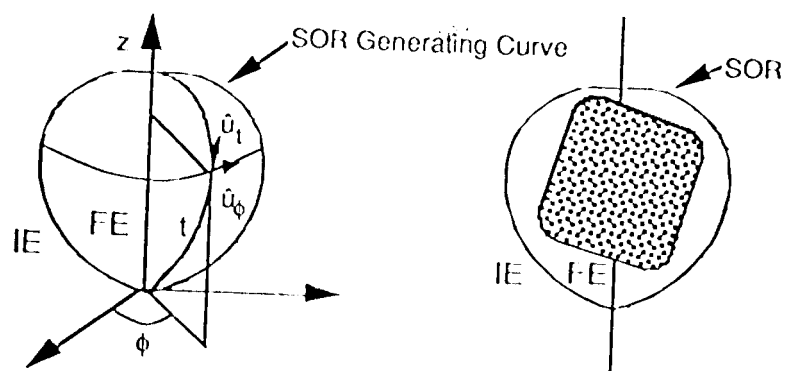
along a generator at 45 degrees.

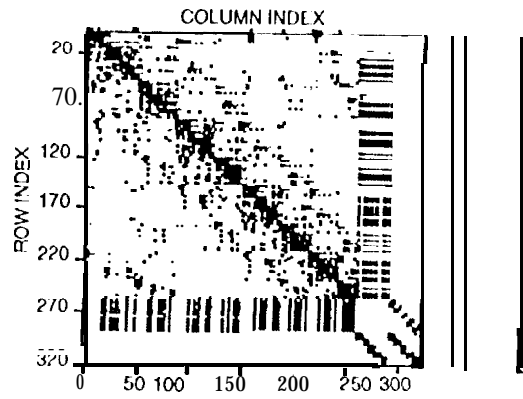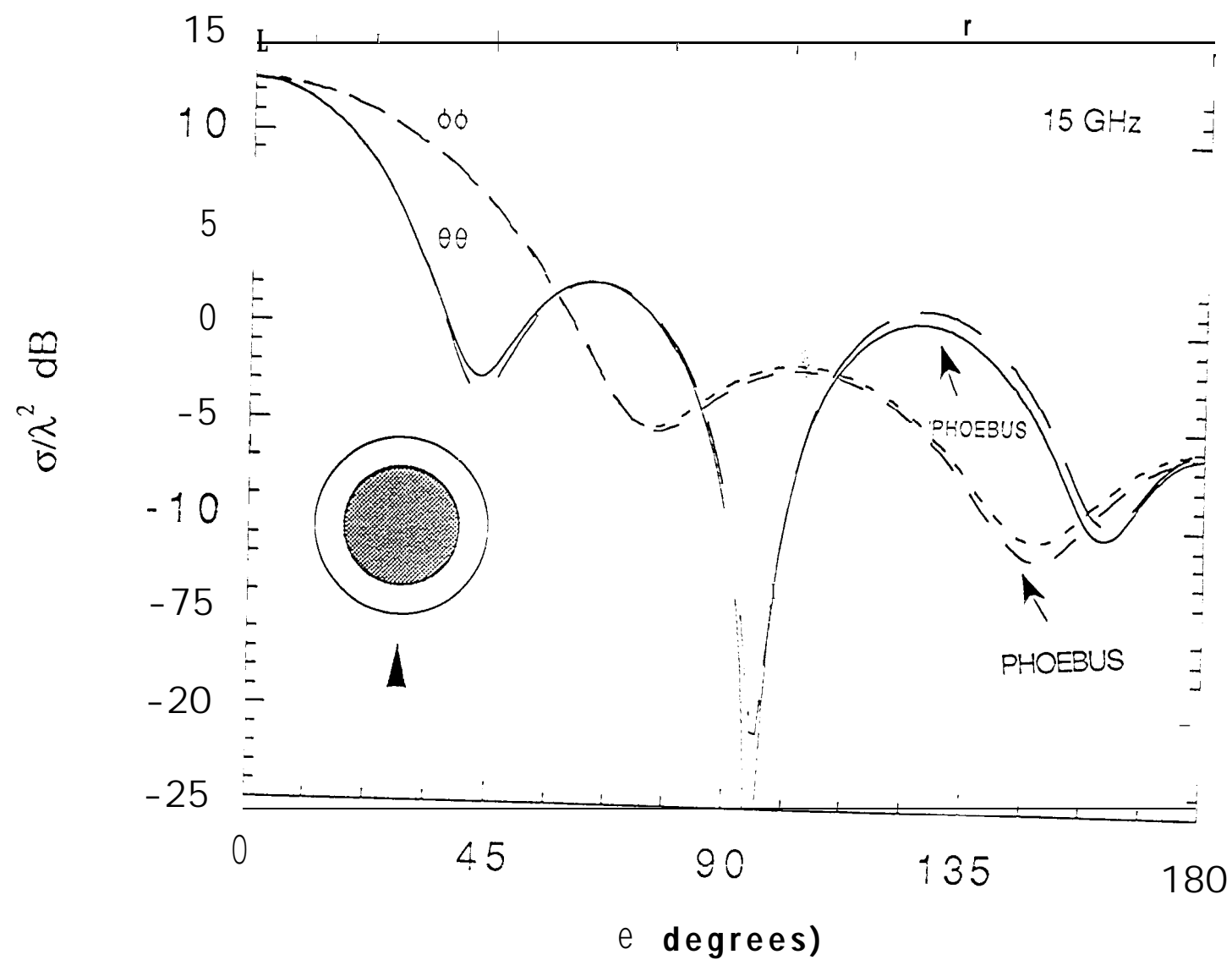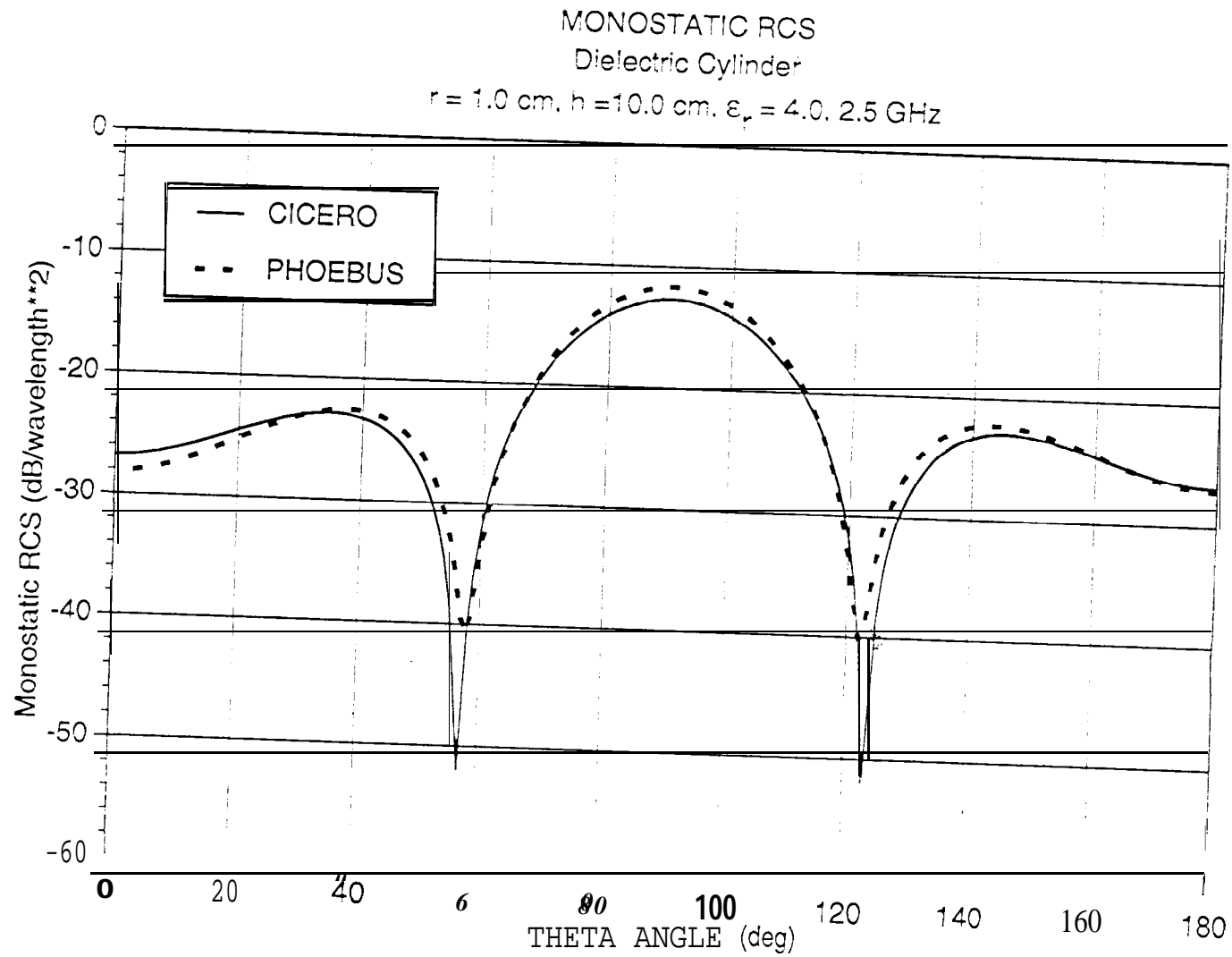Figure 1. Geometry of scatterer showing interior ant] exterior regions.

Figure 2.   Scatter plot figuratively showing structure of system of equations. Darkened spaces indicate non-zero matrix entries.

COATED METAL SPHERE $\varepsilon = 4 - i$

MONOSTATIC RCS
Dielectric Cylinder
$r = 1.0$ cm, $h = 10.0$ cm, $\varepsilon_r = 4.0$, 2.5 GHz

CICERO
PHOEBUS

Monostatic RCS (dB/wavelength**2)

THETA ANGLE (deg)

SURFACE ELECTRIC AND MAGNETIC FIELDS
DIELECTRIC SPHERE